MAUSAM, **54**, 1 (January 2003), 111-120

551.501 : 551.465

Space based techniques for remote sensing of oceanic winds : A Review

ABHIJIT SARKAR

Oceanic Sciences Division, Meteorology & Oceanography Group

Space Applications Centre (ISRO), Ahmedabad, India

e mail : sarkar_abhi2000@yahoo.com

सार – इस शोध पत्र में अंतरिक्ष प्लेटफार्म से नियमित अंतरालों पर भूमंडलीय महासागरों के ऊपर लिए जाने वाले सतही पवनों के प्रेक्षणों के बारे में बताया गया है। इसमें पिछले कुछ दशकों में विकसित की गई विभिन्न तकनीकों पर प्रकाश डाला गया है। सूक्ष्म तरंग प्रकीर्णनमापी सर्वाधिक सफल पवन संवेदक है जो सदिश (वैक्टर) पवनों संबंधी सूचना बिलकुल सही उपलब्ध कराता है। मौसम का पूर्वानुमान करने के लिए वर्ष 2005 में एम.ई.टी.ओ.पी.–1 के आरम्भ होने के साथ प्रकीर्णनमापी नेमी उपग्रह प्रणाली का हिस्सा होगा। संश्लेषित अपरचर रेडार आँकडों से उच्च स्थानिक विभेदन तथा विस्तृत महासागरों और तटीय जलक्षेत्रों दोनों में उपलब्ध पवनों के आँकड़ें पुनः प्राप्त करना शोध प्रयासों में से एक है। इस शोध–पत्र में विकिरणमापीय, तुंगतामापीय और प्रकाशीय पवन मापन तकनीकों की भी समीक्षा की गई है।

ABSTRACT. Observations of surface winds over the global oceans at regular intervals from space platforms have been demonstrated. This paper focuses on different techniques developed over the past few decades. The most successful wind sensor has been the microwave scatterometer, which can provide vector winds with reasonable accuracy. With the launch of METOP-1, scheduled in 2005, scatterometer will be part of routine satellite system for weather forecast. Among the research efforts has been retrieval of winds from Synthetic Aperture Radar data, available in high spatial resolution and in both open oceans and coastal waters. Radiometric, altimetric and optical wind measuring techniques are also reviewed in the paper.

Key words – Scatterometer, Radiometer, Altimeter, SAR, Sun glitter, Remote sensing.

1. Introduction

The ocean is a turbulent global fluid medium with a rich spectrum of motions. Many of these oceanic motions are directly forced by the wind stress at its upper boundary (*i.e*., the ocean surface). Accurate observations of surface wind stress and wind velocity over the oceans are required for a wide range of meteorological and oceanographic applications. Surface winds are essential for now casting weather, and to provide initial conditions and verification data for numerical weather prediction (NWP) models. In addition, surface winds are needed to drive ocean models and surface wave models, to calculate surface fluxes of heat, moisture and momentum, and to construct surface climatologies.

Major ocean currents are strongly wind - dependent. A glaring example is Somali current in the western Indian Ocean. The strength of this current starts increasing along with the reversal of monsoon winds in the Indian Ocean. Large-scale tropical and equatorial current systems are also known to respond predictably to changes in the wind field. The best specific example is the well-known El Nino phenomenon, in which warm water abruptly appears at the eastern boundary of the southern equatorial Pacific. Observational evidence, analytical studies and numerical simulations – all associate El Nino with low frequency variations in the wind. According to the model of El Nino, a large amplitude Kelvin wave in the ocean is excited by a relaxation of the zonal component of the surface winds along the equator which rapidly propagates eastward. When the wave front reaches the coast of South America it deepens the mixed layer and thermocline along the South American coast. This deep surface layer isolates the cold water below initiating coastal warming, causing disastrous consequences.

The need for wind data for specification of initial values in numerical predictions of weather are well known. The data consist of three dimensional fields of horizontal velocities along with temperature and humidity at locations comparable in spatial distribution with the grid points of the numerical models used at frequencies sufficient to capture the variations.

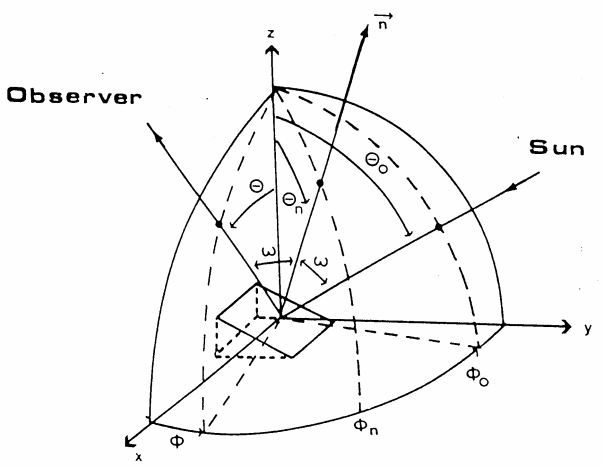

Fig. 1. Reflection geometry. The solar radiation reflects against the wave slope defined by the normal vector **n.** The reflected radiation is observed in the (θ, ϕ) direction

Conventional data fall far short in providing such data either in space or in time. Besides, conventional data for known reasons have land-bias. It is in this context, satellite measurements assume importance. A review of space based techniques is given below.

2. Measurement techniques

The wind stress at the sea is the average turbulent transfer of horizontal momentum from the atmosphere to the ocean by vertical air movements. This transfer is difficult to measure even with a stable observing platform and very sensitive anemometers. The air-sea interface is a hostile environment for sensors. Turbulence time scales are as short as a few seconds and the turbulent velocities are as large as several meters per second, resulting in very few direct stress measurements. Conventional anemometers make measurements at a fixed height (usually 10 m). The surface stress is computed by the well-known "bulk formula".

$$\tau = \rho_A \, C_D \, |V| \, V$$

where ρ_A is air density and C_D is the drag coefficient whose value depends on wind speed and air-sea temperature difference. Unfortunately, the bulk formula approach is not entirely satisfactory.

Developments in space based techniques and technology over the past few decades resulted in significant advancement in observations of winds over the oceans. The most prominent among these is Scatterometric techniques. Space based radiometers and altimeters are other sources of ocean surface wind speed. More recently, Synthetic Aperture Radar data have been used to infer wind fields. Each technique has its own limitation and strength. These techniques are discussed in the following paragraphs.

3. Optical observations

In their early studies, Cox and Munk (1954, 1956) had characterized the ocean surface with the help of observations of sunglint. The sunglint is often regarded as nuisance which is to be avoided. However, there are several studies which exploited the use of sunglint for determination of oceanographic parameters (for example, Stewart, 1985; Khattak *et al.*, 1991; Varma, 1999). Wald and Monget (1983) have derived the following equation for glitter reflectance R_g (Fig. 1) :

$$R_g(\theta,\phi;\theta_0,\phi_0;V) = \frac{\pi r(\omega) P(\theta_n, V)}{4\cos\theta_0 \cos\theta \cos^4 \theta_n}$$

where,

θ , ϕ - observer zenith and azimuth angles,

θ_0, ϕ_0 - sun zenith and azimuth angles,-

ω - the reflection angle,

$r(\omega)$ - the reflection factor computed for a perfectly smooth surface (Fresnel reflection factor).

θ_n, ϕ_n - the components of the normal vector to the slope for which the specular reflection conditions are fulfilled.

From this equation, three methods can be derived to infer surface winds from sun glint observations. The first one deals with absolute value of glitter reflectance after the other sources of radiation have been removed, while the other two methods rely on the geometrical characteristics of the sensed glitter pattern rather than on the brightness values. The second one is based upon the shifting of the brightness point away from its geometrical location for null wind, while the third method measures the broadening of the pattern as the sea roughens. The first method is difficult to use as other sources of radiation are not easy to remove. The second method requires very precise knowledge of the expected and observed position of the centre of the glint. The third method requires relative intensity and distance between two lines of equal intensities.

One exercise over Mediterranean Sea with AVHRR data yielded correlation of 0.7 between sunglint - derived

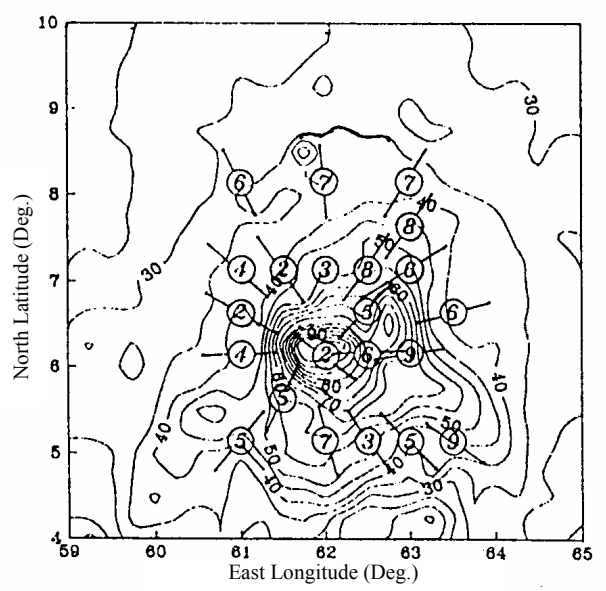

Fig. 2. Iso-intensity plot of sunglitter observed in INSAT-1B VHRR image of 7 August 1987, 0900 UTC. Estimated wind speeds in m/sec in circles

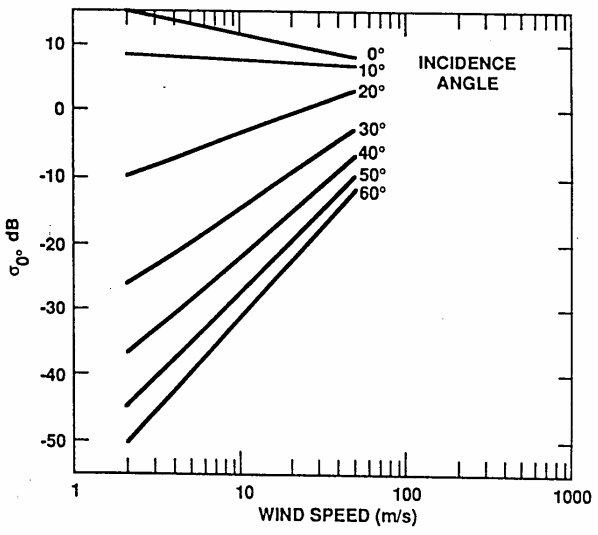

Fig. 3. Ku-band Scatterometer backscattering coefficient variation with near surface wind speed

wind speed and meteorological observations (Khattak *et al*., 1991). Wind speeds were also estimated from INSAT VHRR data (Fig. 2) by the method which relies on the geometrical characteristics of the observed glitter pattern rather than the absolute reflectance values (Prakash *et al*., 1994). The sunglint method however is limited to time and locations of sunglint occurrence. Besides, the sunglint characteristics during high wind speed conditions are complex.

4. Scatterometer

Scatterometry has its origin in early radars used in World War II. The radar measurements over ocean were corrupted by sea clutter (noise) and it was not known at that time that the clutter was the radar response to the winds over the oceans. Radar response was first related to wind in the late 1960's. The first scatterometer flew as part of the Skylab missions in 1973 and 1974, demonstrating that space-borne scatterometers were indeed feasible. The Seasat-A Satellite Scatterometer (SASS) operated from June to October 1978 and proved that accurate wind velocity measurements could be made from space. A single-swath scatterometer flew on the European Space Agency's ERS-1 mission.

The basic measurement made by a scatterometer is σ° (radar backscatter cross section).Wind stress over the ocean generates waves which roughen the sea surface. Changes in wind velocity cause changes in surface roughness, which in turn modify the radar cross section of the ocean and hence magnitude of backscattered power.

The relationship between σ° and near surface wind velocity is known as the "geophysical model function" and has been the subject of intense study over the past three decades. Various theoretical studies have been advanced to explain the sensitivity of σ° on surface wind speed and direction, and parameters, related to geometry of observation. Using the phenomenon of Bragg Scattering, the well known Two-Scale Scattering theory provides the following expression for σ° (Ulaby, *et al*., 1982, Fung and Lee, 1982, Sarkar and Kumar, 1986) :

$$\sigma^0_{pp}(\theta,\phi) = \int_{-\infty}^{\infty}\int_{-\infty}^{\infty} \sigma_{pp}(\theta,\phi)\, P_\theta\,(Z_{x'}, Z_{y'})\, dZ_x\, dZ_y$$

where,

σ_{pp} is backscattering coefficient for polarisations *pp*;

θ is the incidence angle; ϕ is the aspect angle;

Zx Zy are the slopes in x and y directions.

Essentially, the maximal backscatter is provided by those ocean surface waves which satisfy the Bragg resonance condition, and these are generally wind-induced capillary or gravity waves. Modern scatterometer parameters are selected to respond to capillaries.

While significant progress in theories has been made, the gaps in our knowledge remain formidable.

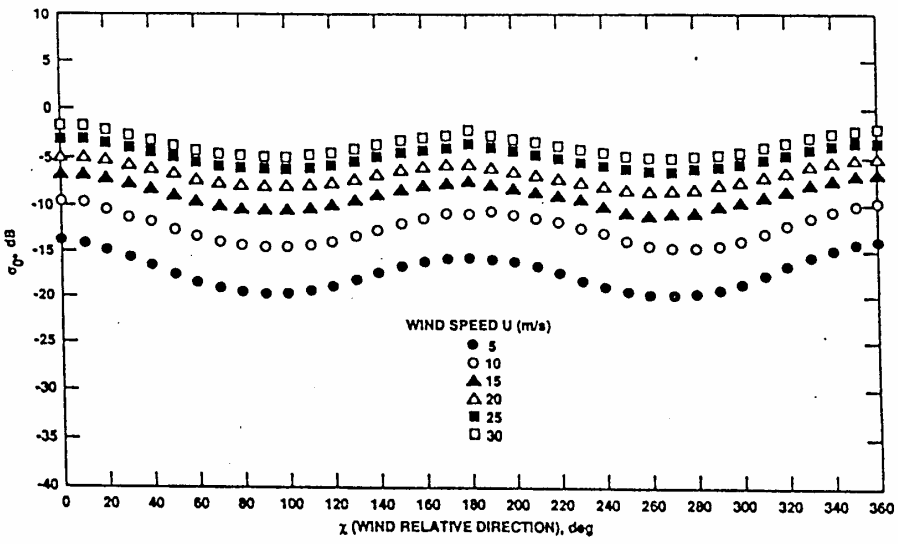

Fig. 4. Ku-band Scatterometer backscattering coefficient variation with relative wind direction

Lacking rigorous theoretically based expressions, empirical models have been established to relate ocean radar cross section and near-surface wind. Figs. 3&4 represent schematically the model function for Ku-band VV-pol (based on Seasat scatterometer data). Although difficult to detect in Fig. 4, there is also a small but significant difference in σ° between upwind and downwind angles (known as the "upwind-downwind asymmetry"), with upwind cross sections being typically larger than downwind. The upwind-downwind asymmetry increases with increasing incidence angle, is larger for HH-pol than for VV-pol radiation, and is larger at lower wind speeds. Although small, this asymmetry is critical; in its absence, scatterometer vector wind measurements would always result in an ambiguity of 180° (Naderi *et al*., 1991).

The retrieval algorithm for vector winds of a scatterometer yields multiple solutions of wind vector (Fig. 5) along with their priority in identifying the true wind vector from a given set of radar backscatter measurements. Under noise-free (ideal) conditions, the highest priority solution always represents the true wind vector but for realistic data (usually noisy), it is not so all the time. Most of the times, however, the true direction is contained in the first two highest priority solutions. This ambiguous direction over a swath is removed by a method based on 'trend' or 'consensus' of the highest priority wind direction solutions over that area. A median filtering approach has been successfully used to remove these ambiguities (Gohil, 1992; Gohil and Pandey, 1985) with the help of a median window. With a moving window of optimized size, median wind direction at each location is determined. This is used to select the direction

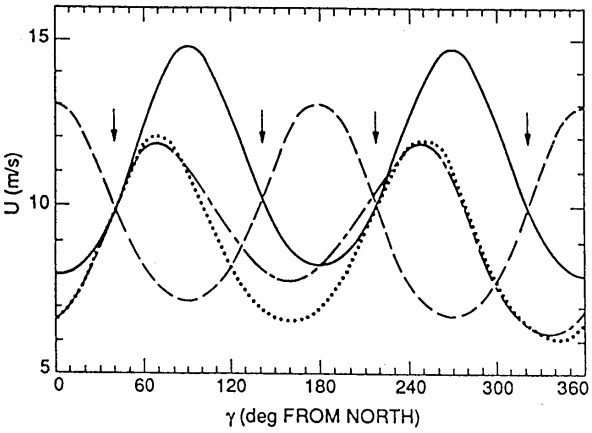

Fig. 5. Loci of possible vector winds associated with co-located noise-free σ_0 measurements obtained from antennas at various azimuth angles. Heavy solid line : antenna angle of 0° (v-pol); dashed line : angle of 90° (v. pol); light solid line : angle of 25° (v. pol); dotted line; angle of 25° (h-pol). Arrows indicate solutions obtained using only the antennas at 0° and 90°

closest to it. Data of the entire swath thus processed produces the unambiguous wind field.

The NASA Scatterometer (NSCAT), launched aboard Japan's ADEOS-Midori Satellite in August 1996, was the first dual-swath, Ku-band scatterometer to fly since Seasat. From September 1996 till June 1997, NSCAT performed flawlessly and returned a continuous stream of global sea surface wind vector measurements. Because of the success of the short-lived NSCAT mission, future Ku-band scatterometer instruments are now greatly anticipated by the ocean winds user community.

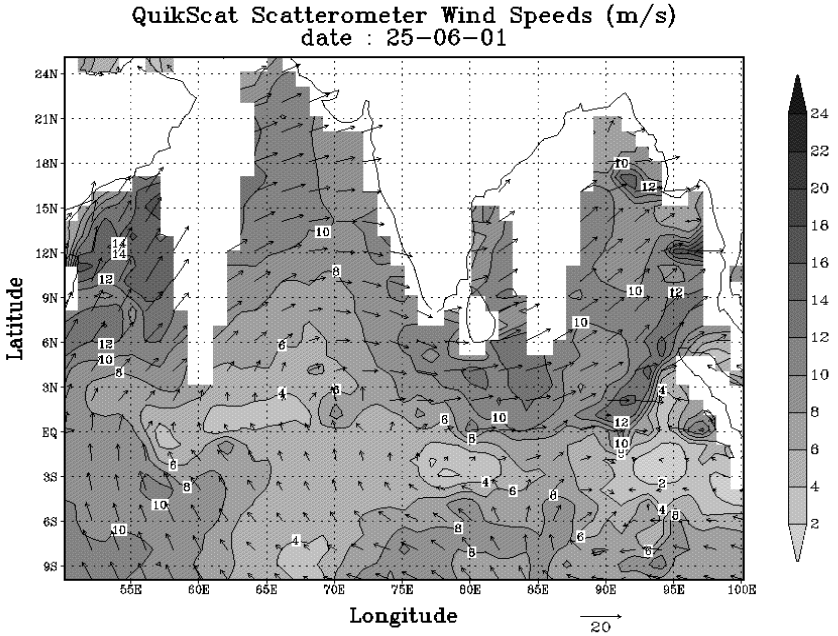

Fig. 6. Quikscat wind fields

The NSCAT mission proved so successful, that plans for a follow-on mission were accelerated to minimize the gap in the scatterometer wind database. The Quikscat mission launched SeaWinds scatterometer in June 1999. Fig. 6 shows how well the monsoon wind fields are reproduced by Quikscat scatterometer.

5. Synthetic aperture radar

It is only recently that remote sensing has offered the routine, all weather capability of systematically measuring winds at sub-kilometer scale resolution. Space-borne synthetic aperture radar (SAR) imagery of the ocean surface reveals high-resolution patterns of wind speed and direction variations. These patterns offer the attractive prospect of measuring surface winds from space in coastal regions. It is precisely in coastal regions where high-resolution wind speeds are both necessary and particularly difficult to measure from space. It has been convincingly demonstrated (Monaldo, 2000) that Radarsat SAR can be processed into estimates of wind speed sufficiently quickly and accurately to be useful operationally.

The challenge in estimating wind speed from SAR radar cross section measurements is two fold. First, one must be able to specify the relationship between ocean surface wind velocity and normalized radar cross section (NRCS) - the geophysical model function (GMF). The second, The SAR directly measures only backscattered power from which NRCS is to be determined. Unfortunately, the relationship between NRCS and wind speed is not unique. For any measured cross section there are a variety of combinations of wind speed and direction that will produce the same value of radar cross section. Space-borne scatterometers resolve this ambiguity by measuring the surface cross section at a number of aspect angles and polarizations (discussed in the section on scatterometery). However, scatterometer technology permits spatial resolutions of only 25-50 km, applicable more to the open ocean than to coastal areas. This uniqueness problem can be resolved in SAR imagery if an estimate of wind direction is provided. One possible way is to use the spatial variation in the cross sections caused by waves as a way to measure wind direction from the SAR imagery itself. Although such signatures definitely exist, they do not exist all the time. A more popular way has been adapting the wind direction estimates from numerical forecast models. Therefore, for an operational procedure to work, there must be a ready source of model wind direction estimates. A Naval Operational Global Atmospheric Prediction System (NOGAPS) was used for this purpose. Comparisons of SAR-derived wind speeds with those measured by buoy indicate that a properly calibrated SAR can be used over the ocean as high spatial resolution anemometer. The standard deviation in wind speed retrievals is as low 1.76 m/s.

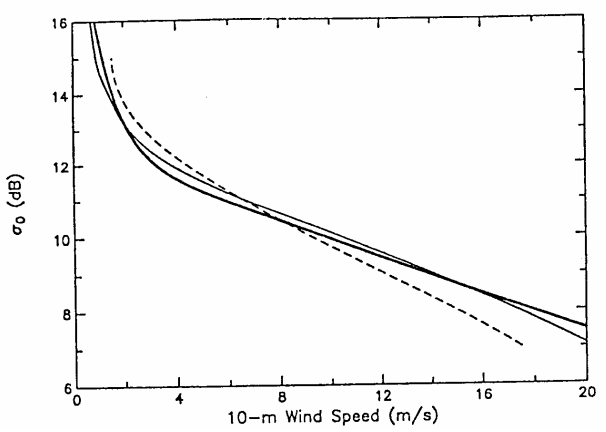

Fig. 7. A comparison of empirical model functions for altimeter estimates of wind speed at a height of 10 m above the sea surface. The three curves correspond to the Smoothed Brown (dashed line), the Modified Chelton and Wentz (thin solid line) and the Freilich and Challenor (heavy solid line) Model functions

The development and launch of the C-band, VV-polarization (VV-pol) wind scatterometer aboard the ERS-1 satellite necessitated the development of a well-validated scatterometer GMF for this system. At present the most commonly used GMF is CMOD4 GMF (Stoffelen and Anderson, 1993) that specifies the VV-pol NRCS,

$$\sigma_v^0 = a(\theta) U^{\gamma(\theta)} [1 + b(\theta)\cos\phi + c(\theta)\cos 2\phi]$$

When the radar is looking into the wind (ϕ=0), $\sigma°$ is maximum. Since $\gamma(\theta) > 1$, the above equation indicates that the NRCS increases with wind speed. There is no validated scatterometer geophysical model function that relates the HH polarisation NRCS of the RADARSAT–SAR to wind. To deal with this deficiency, a polarisation ratio relating the HH-pol NRCS was developed (Monaldo *et al*., 2001).

6. Altimeters

In addition to measuring the time delay and shape of the returned pulse for estimating respectively, the range and $H_{1/3}$, the altimeter also measures the power of the returned signal, which is related to the wind-induced roughness of the sea surface. The power measurement is not direct, however. The physics of the relation between wind speed and altimeter measurements of $\sigma°$ are different from the Bragg scattering mechanism responsible for the backscattered power at the 20-60° incidence angles measured by a scatterometer. At the small incidence angles relevant to altimetry (less than 1° from satellite nadir), the backscattered power results almost totally from specular reflection from favourably oriented facets with wavelengths longer than about three times that of the incident radiation (Brown, 1990). As the wind speed increases, the sea-surface roughness increases and a greater fraction of the incident radiation is reflected away from the satellite. Altimeter measurements of $\sigma°$ are therefore inversely related to wind speed. There is no significant dependence of $\sigma°$ on wind direction at small incidence angles so only the wind speed can be inferred from altimetry.

Historically, altimeter wind-speed model functions relate $\sigma°$ to the neutral-stability wind speed at a height of 10 m above the sea surface. Although a theory-based model function for altimeter estimates of wind speed has recently been developed by Elfouhaily *et al*. (1998), the model functions used most widely to date have been purely empirical.

A so called 'Smoothed-Brown' polynomial model function was built up by Goldhirsh and Dobson (1985) and Dobson *et al*., (1987), which was widely used to infer wind speed from altimeter $\sigma°$ measurements. Collection of an adequate *in situ* database from which to develop an accurate empirical wind speed model function will always be a problem. This is especially true for altimetry which measures $\sigma°$ for only a small area (a footprint diameter less than 10 km) at satellite nadir. Chelton and Wentz (1986) utilized the simultaneous measurements of $\sigma°$ by the Seasat altimeter and the Seasat-A Satellite Scatterometer (SASS) to obtain a greatly expanded calibration data set for deriving a wind speed model function (denoted as the CW model function hereafter) for the Seasat altimeter. The CW model function was derived in tabular form by comparison of altimeter measurements of $\sigma°$ with 241,000 SASS observations of wind speed at 24° incidence angle. The clear advantage of a SASS-based altimeter wind-speed model function is the much larger calibration database spanning a broader range of wind speeds than could ever practically be obtained from buoy observations over the lifetime of a single altimeter mission. The SASS wind speed used to derive the CW model function were extensively compared with buoy observations and found to have an rms accuracy of better than 1.6 m sec^{-1} with negligible bias over the range. It should be noted, however, that the dependence of $\sigma°$ on wind speed is very flat for higher wind speed regime (Fig. 7). Altimeter estimates of wind speed are therefore most sensitive to errors in $\sigma°$ at high wind speeds. It will never be possible to measure high wind speeds as accurately from an altimeter as from a scatterometer.

To circumvent the limited availability of coincident buoy and altimeter estimates of high wind speeds, Freilich and Dunbar (1993) proposed the use of wind speeds estimated by numerical weather prediction (NWP) models to create a large database from which a model function for altimeter estimates of wind speed could be derived.

Freilich and Challenor (1994) proposed a fundamentally different approach for deriving a wind speed model function that obviates the need for collocated altimeter measurements of $\sigma°$ and buoy or NWP estimates of wind speed. They showed that the relationship between wind speed and $\sigma°$ can be determined solely from the separate, rather than joint, probability density functions of wind speed and $\sigma°$. The only requirements is that $\sigma°$ vary monotonically and uniquely with all available observations. By eliminating the need for collocated altimeter and buoy observations, this probabilistic approach address the most fundamental limitation of model function development. Denoting the cumulative probability density functions for wind speed and $\sigma°$ as Γ_U and $\Gamma_{\sigma o}$ respectively, Freilich and Challenor (1994) showed that the wind speed U is related to the probability distribution functions by

$$U = \Gamma_U^{-1} \left[1 - \Gamma_{\sigma 0}(\sigma_0)\right]$$

Where Γ_U^{-1} is the inverse function of Γ_U, *i.e*., the value of the cumulative probability density function corresponding to the particular value of the wind speed U. Because Γ_U is monotonic, such an inverse function is assured to exist. They applied the formulation to one year of Geosat data. The wind speed distribution function was determined from both buoy data and NWP wind-speed estimates.

The Freilich and Challenor (1994) NWP-based "geometric" model function (referred to here as the FC model function) can be accurately expressed analytically by

$$\sigma_0 = 12.40 - 0.2459U + 8.956 \exp(-0.9593U)$$

where U is the wind speed at 10 m. As shown in Figure 8, the FC and MCW model functions agree to within 1 m sec^{-1} for wind speeds over the full range of $\sigma°$ values.

Elfouhaily *et al*. (1998) have recently presented a theoretically based method for estimating surface wind speed form linear combinations of K_u-band and C-band measurements of $\sigma°$ by the T/P dual-frequency altimeter. The basis for the approach is that the difference between $\sigma°$ at the two frequencies is related to the spectrum of short gravity waves with wavelengths in the range responsible for the difference in the backscatter at the two frequencies. As noted previously, Brown (1990) showed that the backscattered power from radar measurements at nadir results almost totally from specular reflection from wavelength longer than about three times that of the incident radiation (*i.e.* wavelengths longer than about 6 and 16 cm for the K_u-band and C-band frequencies, respectively). The short gravity waves with wavelengths of 6-16 cm are closely coupled to the wind stress at the surface (and hence the friction velocity). Elfouhaily *et al*. (1998) derived a theoretical relationship between the surface friction velocity and the two $\sigma°$ measurements based on a prescribed wave spectrum.

The estimates of friction velocity were then transformed into the neutral-stability wind speed at 10 m height using a sea-state dependent drag law. With the sea-state characterized by the pseudo wave age computed from wind speed itself, the wind speed must be estimated iteratively.

From comparison with collocated buoy data, Elfouhaily *et al*. (1998) showed that the accuracy of their theory based wind speed estimates (referred to here as the E98 model function) was somewhat better than the empirical wind speed model functions.

In summary, there is remarkable agreement between empirical and theoretical model functions for altimeter estimates of wind speed. The MCW, FC and E98 model functions are all in close agreement for wind speeds up to 15 m sec^{-1}. The rms errors of the three model functions are 1.5 - 1.75 m sec^{-1} with biases of less than 0.5 m sec^{-1}. Elfouhaily *et al*. (1998) found that the E98 wind speed estimates were more consistent with a model for hurricane winds than were the MCW wind speed estimates.

7. Passive microwave radiometer

While most satellite-based attempts to measure ocean surface winds from space have involved, active radar instruments, usually scatterometers (Seasat, ERS I & II, Quikscat), considerable success has also been achieved using passive radiometers to retrieve the magnitude of these winds. The radiative emission from the ocean surface of energy in microwave band is strongly dependent on surface geometry parameters. Correspondingly, the wind field at the ocean surface plays a significant causal role in the shaping and evolution of these surface parameters. This relationship has been exploited over the past three decades by a variety of microwave remote sensing techniques in an effort to better determine ocean surface winds through airborne and

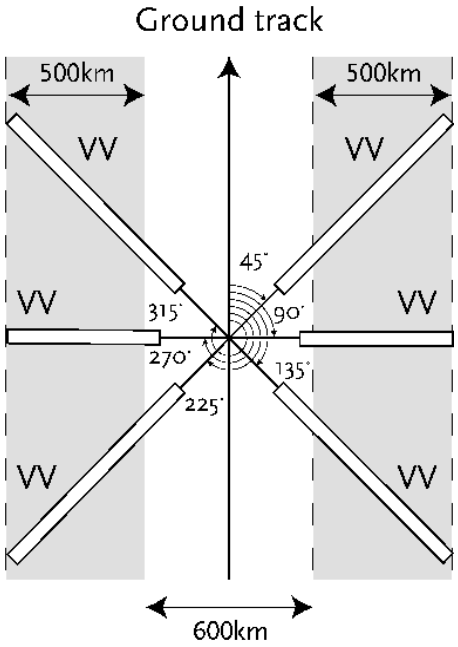

Fig. 8. METOP – 1 ASCAT geometry

spaceborne measurements of the surface radiated microwave energy (Connor and Chang, 2000).

The SSM/I is a series of Earth observing multiband microwave radiometers operating on Defense Meteorological Satellite Program (DMSP) polar orbiters. Since July 1987, five SSM/I s have been providing data (F08, F10, F11, F13, F14). The SSM/I data are processed under NASA's Pathfinder program using an algorithm that is based on a model for the brightness temperature of the ocean and the intervening atmospheric (Wentz, 1997) using five channels (19 & 37 GHz V & H and 22 GHz V). The algorithm can simultaneously retrieve with high precision, wind speed at 10 m besides columnar water vapour and liquid water. Thus this is a longest time series of satellite based wind speed measurements. A detailed validation study with 10 year SSM/I data was carried out by Goodberlet *et al*. (1990), Mears *et al*. (2001), Meissner *et al*. (2001) showing typically standard deviation < 1.4 m/s with respect to buoys, and 2.1 – 2.4 m/s with respect to model reanalyses. The TMI on TRMM is a nine-channel passive microwave radiometer based upon the SSM/I with key differences of added pair of dual polarised 10.7 GHz channels and a change of the water vapour channel from 22.235 to 21.3 GHz (Kummerow *et al*., 1998). The studies on variability of surface winds and SST derived from TMI during monsoon seasons, in conjunction with *in situ* data revealed enormous potentiality of TMI data (Parekh *et al*., 2002). Multifrequency Scanning Microwave Radimeter (MSMR) aboard the Indian satellite IRS P4 was launched in May 1999. MSMR is four frequency (6.6, 10.65, 18.0 and 21.0 GHz) dual – polarisation sensor, was placed on a sun synchronous orbit (Misra *et al*., 2002). The ocean surface wind speed along with sea surface temperature, integrated water vapor and cloud liquid water were derived by the radiative transfer based statistical algorithm (Gohil *et al*., 2000) and subjected to geophysical valiation (Ali , 2000). MSMR data was widely used by meteorological and oceanographic community for monsoon and ocean state related studies. Nystuen *et al*. (1993) and Varma *et al*. (1998) compared SSM/I winds with those from Geosat altimeter and found them to be consistent, particularly for winds upto 12 m/s. Varma *et al*. (2002) carried out extensive inter-comparison exercises of wind speeds derived from MSMR, SSM/I and TMI radiometers. More than 70% of the difference of the wind speed derived from MSMR and the other sensors are seen to be within 3 m/s.

8. Future perspective

Metop-1, Europe's first operational polar-orbiting weather satellite carrying an Advanced Scatterometer 'ASCAT' and a set of 'heritage' sensors, is scheduled for launch in 2005. With an overall mass of about 4.5 tons, Metop will nominally fly at 835 km altitude in a 5-day repeat sun-synchronous orbit with an Equator descending crossing time at 9.30 am. NOAA will continue to operate its afternoon satellite service from a complementary orbit, which follows a track at a local solar time of 14:30. The measurement geometry of the ASCAT aboard the Metop satellites will be similar to those of the C-band wind scatterometers of ERS-1 and ERS-2 but it will have a swath on each side of the ground track, doubling the coverage of ERS-1/-2. Each swath is covered by three antennae looking 45 degrees forwards (fore-beam), sideways (mid-beam), and 45° backwards (aft-beam) with respect to the satellite flight direction. The incidence angle ranges from 25° to 55° for the mid-beam and from 34° to 65° for the fore and aft-beams. Depending on the processing, the spatial resolution will be 25 or 50 km both along and across-track. The microwave frequency will be 5.255 GHz and only vertical polarisation (VV) will be used. Each swath is about 300 km off the ground track and 500 km wide, as indicated in the graphic (Fig. 8).

Apart from the new generation scatterometer and radiometer measurements of oceanic winds, innovative method of synergising active and passive microwave sensor data have been developed. Jones *et al*., (2002) have shown the capability of determining wind vectors from TRMM Microwave Imager and Precipitation radar data for this purpose.

References

Ali, M. M., 2000, "Validation of MSMR geophysical data products", Proc. PORSEC-2000, Goa, 182-191.

Brown, G. S., 1990, "Quasi specular scattering from air-sea interface", in "Surface waves and fluxes", **2**, 1-39, (Eds Gernaert GL and Plant WJ), Kluwer.

Chelton, D. B. and Wentz, F. J., 1986, "Further development of an improved altimeter wind speed algorithm", *J. Geophys. Res.*, **91**, 14250-14260.

Connor, L. N. and Chang, P. S., 2000, "*IEEE Trans Geosci. & Rem. Sen*.", **38**, 2009-2016.

Cox, C. and Munk, W., 1954, "Measurements of the roughness of the sea surface from the photographs of the sun glitter", *J. Opt. Soc. Am*., **44**, 838-850.

Cox, C. and Munk, W., 1956, "Slopes of the sea surface deduced from photographs of sun glitter", *Bull. Scripps Inst. Oceanogr*., **6**, 401-488.

Dobson, E. B., Monaldo, F., Goldhirsh, J. and Wilkerson, J., 1987, "Validation of GEOSAT altimeter derived wind speeds and significant wave heights using buoy data", *J. Geophys. Res.*, **92**, 10719-10732.

Elfouhaily, T., Vandemark, D., Gourrion, J. and Chapron, B., 1998, "Estimation of wind stress using dual frequency TOPEX data", *J. Geophys. Res.*, **103**, 25101-25108.

Freilich, M. H. and Challenor, P. G., 1994, "A new approach for determining fully empirical altimeter wind speed model functions", *J. Geophys. Res.*, **99**, 25051-25062.

Freilich, M. H. and Dunbar, R. S., 1993, "Derivation of satellite wind model functions using operational surface wind analyses: An altimeter example", *J. Geophys. Res.*, **98**, 14633-14649.

Fung, A. K. and Lee, K. K., 1982, "A semi empirical sea spectrum model for scattering coefficient estimation", *IEEE J. Ocean Engg*., **7**, 166.

Gohil, B. S. and Pandey, P. C., 1985, "An algorithm for retrieval of oceanic wind vectors from the simulated SASS normalised radar cross-section measurements", *J. Geophys. Res*., **90**, 7307-7311.

Gohil, B. S., 1992, "Extraction of ocean surface wind field from simulated ERS-1 scatterometer data", *Int. J. Rem. Sen*., **13**, 3311-3327.

Gohil, B. S., Mathur, A. K. and Varma, A. K., 2000, "Geophysical parameter retrieval over global oceans from IRS P4/MSMR", Proc. PORSEC-2000, Goa, 207-211.

Goldhirsh, J. and Dobson, E. B., 1985, "A recommended algorithm for the determination of ocean surface wind speed using a satellite-borne radar altimeter", Rep. JHU/APL SIR-85-U005, Johns Hopkins Univ., Laurel, MD.

Goodberlet, M. A., Swift, C. T. and Wilkerson, J. C., 1990, "Ocean surface wind speed measurements of the Special Sensor Microwave/Imager (SSM/I)", *IEEE Trans. Geosci. and Remote Sens*., **28**, 823-828.

Jones, W. J., Soisuvarn, S., Park, J., Adams, I. and Kasparis, T., 2002, "Combined active and passive microwave sensing of ocean surface wind vector from TRMM (personal communication)".

Khattak, S., Vaughan, R. A. and Cracknell, A. P., 1991, "Sunglint and its observation in AVHRR data", *Remote Sensing of Environment*, **37**, 101-116.

Kummerow, C., Barnes, W., Kozu, T., Shiue, J. and Simpson, J., 1998, "The TRMM Sensor Package", *JAOT*, **15**, 809-817.

Mears, C. A., Smith, D. K. and Wentz, 2001, "Comparison of SSM/I and buoy measured wind speeds from 1987-1997", *J. Geophys. Res.*, **106**, 11719-11729.

Meissner, T., Smith, D. and Wentz, F., 2001, "A 10-year intercomparison between collocated SSM/I oceanic surface wind speed retrievals and global analyses", *J. Geophys. Res.*, **106**, 11713-11742.

Misra, T., Jha, A. M., Putrevu, D., Rao, J., Dave, D. B. and Rana, S. S., 2002, "Ground calibration of multifrquency scanning microwave radiometer (MSMR)", *IEEE Trans*, **40**, 504-508.

Monaldo, F., 2000, "The Alaska SAR demonstration and near-real-time Synthetic Aperture Radar winds", Johns Hopkins APL Technical Digest, **21**, 75-79.

Monaldo, F. M., Donald, R. T., Beal, R. C., Pichel, W. G. and Clemente-Colon, P., 2001, "Comparison of SAR-derived wind speed with model predictions and ocean buoy measurements", *IEEE Trans. Geo. Rem.*, **39**, 12, 2587-2600.

Naderi, F. M., Freilich, M. H. and Long, D. G., 1991, "Spaceborne radar measurement of wind velocity over the ocean – An overview of the NSCAT scatterometer system", *Proc. IEEE*, **79**, 850-866.

Nystuen, J. A., Lilly, J. E. and Goroch, A. K., 1993, "A comparison of wind speed measured by the SSM/I and the Geosat altimeter", *Int. J. Rem. Sen.*, **14**, 745-756.

Parekh, A., Sarkar, A., Shah, S. and Narayanan, M. S., 2002, "Comparative studies of SST and wind speed over north Indian Ocean measured with TRMM microwave imager", Scientific Report, MT-SR/06,2002, SAC.

Prakash, W. J., Varma, A. K. and Bhandari, S. M., 1994, "An algorithm for the precise location of the solar specular reflection point in the visible band images from geostationary meteorological satellites", *Computers & Geosciences*, **20**, 1467-1482.

Sarkar, A. and Kumar, R., 1986, "A new semi-empirical sea spectrum for estimating the scattering coefficient", *Int. J. Rem. Sen*., **7**, 1369-1375.

Stewart, R. H., 1985, "Methods of satellite oceanography", University of California Press, Berkley.

Stoffelen, A. and Anderson, D. L. T., 1993, "ERS-1 scatterometer data characteristics and wind retrieval skill", *Adv. Space Res*., **13**, 553-560.

Ulaby, F. T., Moore, R. K. and Fung, A. K., 1982, "Microwave Remote Sensing : Active and Passive", Reading.

Varma, A. K., 1999, "Remote sensing studies on some aspects of ocean environment", Ph.D. Thesis, BHU, Varanasi.

Varma, A. K., Gairola, R. M., Basu, S., Singh, K. P. and Pandey, P. C., 1998, "A comparative study of near concurrent DMSP-SSM/I and Geosat-altimeter measurements of surface winds over the Indian oceanic region", *Int. J. Remote Sens*., **19**, 717-730.

Varma, A. K., Gairola, R. M., Mathur, A. K., Gohil, B. S. and Agarwal, V. K., 2002, "Intercomparison of IRS P4 MSMR derived geophysical products with DMSP-SSM/I and TRMM-TMI finished products", *Proc. Ind. Acad. Sci. (EPS).,* **111**, 247-256.

Wald, L. and Monget, J. M., 1983, "Sea surface winds from sun glitter observations", *J. Geophys. Res*., **88**, 2547-2555.

Wentz, F.J., 1997, A well calibrated ocean algorithm for SSM/Image, *J. Geophys. Res.*, **102,** 8703-8718..